Morphological traits, niche-environment interaction and temporal changes in diatoms

Loïck Kléparski, Gregory Beaugrand, Martin Edwards, François Schmitt, Richard R Kirby, Elsa Breton, F. Gevaert, Emeline Maniez

Morphological traits, niche-environment interaction and temporal changes in diatoms

Loïck Kléparski [1, 2 *], Grégory Beaugrand [1 *], Martin Edwards [3, 4]

François G. Schmitt [1], Richard R. Kirby [5], Elsa Breton [1], François Gevaert [1], Emeline Maniez [1]

[1] Univ. Littoral Côte d'Opale, CNRS, Univ. Lille, UMR 8187 - LOG - Laboratoire d'Océanologie et de Géosciences, F-62930 Wimereux, France

[2] Marine Biological Association, Citadel Hill, Plymouth PL1 2PB, United Kingdom.

[3] Plymouth Marine Laboratory, Prospect Place, Plymouth, PL13DH, United Kingdom.

[4] University of Plymouth, School of Biological and Marine Sciences, Drake Circus, Plymouth, United Kingdom.

[5] The Secchi Disk Foundation, Kiln Cottage, Gnaton, Yealmpton, PL8 2HU, United Kingdom.

* corresponding authors: loick.kleparski@hotmail.fr

Authors' contributions: L.K and G.B designed the study. L.K, G.B and E.M performed the analyses. L.K and G.B wrote the first draft and L.K, G.B, M.E, F.S, R.K, E.B, F.G and E.M discussed the results.

Competing interests: The authors declare no competing interests.

Keywords: annual diatom succession, cell elongation, ecological niche, morphological traits, phenology, North Sea, CPR survey.

Abstract

Annual phytoplankton succession is a key ecological phenomenon that drives marine species' life cycles and energy flows within marine ecosystems. Identifying processes that control annual succession is critical to anticipate climate-induced environmental perturbations of this phenomenon and the consequences upon ecosystem functioning. Here, we demonstrate that diatoms in the North Sea undergo strong morphological changes throughout the year and that species with similar phenology possess comparable morphological traits (e.g. cell elongation) and ecological niches. The spring and autumn periods appear to be dominated by oblates (flattened cells) whereas the summer period is dominated by prolate (elongated cells). Elongation of the cell shape enhances buoyancy and confers a selective advantage in stratified low-nutrient waters typical of summer without changing a diatoms' surface area/volume ratio or its ability to absorb nutrients. Diatom shape thus appears to have evolved as a key adaptation to a specific environment and confers upon a species its specific niche and phenology, and therefore its place in the sequence of annual succession. As a result, shape influences temporal changes in the abundance of diatoms and their putative response to environmental forcing. We suggest that biogeochemical and earth-system models should include diatom cell shape as a parameter in order to improve model predictions and help our understanding of the consequences of climate change on marine ecosystems.

1. Introduction

Diatoms are a major phytoplankton clade that have evolved during the Middle Triassic when sea levels were rising and continental margins were flooding (Falkowski et al., 2004). Diatoms' subsequent increase in diversity during the mid-Cenozoic Era strongly influenced the global carbon cycle (Katz et al., 2005). Today, diatoms account for about 40% of total marine primary production and almost 40% of total particulate organic carbon exported to the deep ocean annually (Jin et al., 2006; Nelson et al., 1995; Tréguer et al., 2018). Annually, the abundance of diatoms rises and falls on

a seasonal basis following a predictable pattern named “Annual Diatom Succession” (called hereafter ADS).

In the North Sea, ADS is characterised by the succession of various species throughout the year, with species such as *Skeletonema costatum* and *Thalassiothrix longissima* dominating in spring, *Guinardia striata* and *G. flaccida* in summer and *Poroboscia indica* and *Bidulphia alternans* in autumn (Caracciolo et al., 2021). ADS therefore determines the pulses of energy that influence the dynamics of the whole marine ecosystem, the life cycle of many zooplankton and fish being coupled with the peaks in primary production or species dominance (Cushing, 1990; Platt et al., 2003). Recently, anthropogenic climate change has begun to alter diatom phenology and biogeography, and this is likely to have strong consequences on trophic interaction and ecosystem functioning (Chivers et al., 2017; Edwards and Richardson, 2004).

To predict the future consequences of climate change on marine ecosystems, we need to i) better understand how diatom communities naturally form and reorganise at multiple time-scales and ii) to identify the key elements and processes that control phenology. Morphological traits (i.e. cell size and shape) are known to play an important role in diatom succession because they influence resource uptake, buoyancy and predation, which are all properties that may explain seasonal changes in species dominance (Behrenfeld, 2010; Caracciolo et al., 2021; Karp-Boss and Boss, 2016; Margalef, 1978; Naselli-Flores et al., 2021; Naselli-Flores and Barone, 2011). The niche of a species (i.e. the set of environmental parameters that enable a species to grow, maintain and reproduce) is also of paramount importance as it controls the range of environmental conditions that a species can tolerate (Hutchinson, 1957). Here, we investigate the relationships between species’ morphological traits (size and shape), ecological niches, and phenology with the aim of identifying the key elements and processes responsible for ADS.

2. Materials and Methods

2.1. Biological data

We used abundance data of 45 diatom species/taxa commonly sampled by the Continuous Plankton Recorder (CPR) survey in the North Sea (51°N, 60°N, -3°E, 9°E; Supplementary Figure S1) between 1958 and 2017 (Reid et al., 2003). This long-term plankton monitoring programme has collected plankton on a monthly basis in the extratropical regions of the North Atlantic Ocean and its adjacent seas since 1946. The sampling machine is a high-speed plankton recorder towed behind voluntary merchant ships at a depth of approximately 7 m (Beaugrand et al., 2003; Reid et al., 2003) (see Supplementary Text S1 for an overview of the CPR limitations and Supplementary Text S2 for CPR data availability)(Beaugrand et al., 2003; Reid et al., 2003). Each value of abundance corresponds to a number of cells per CPR sample, which corresponds on average to 3 m^3 of seawater filtered (Jonas et al., 2004). We calculated a daily climatology of the abundance of 45 diatoms sampled by the CPR survey. To account for all CPR samples collected between 1958 and 2017, we based our climatology on 366 days. We applied twice a 6-order simple moving average on the matrix (366 days x 45 species/taxa) and standardized the abundance data between 0 and 1 for each species, following the procedure described in Caracciolo and colleagues (Caracciolo et al., 2021).

2.2. Environmental data

Supplementary Text S2 provides key references and internet sites for each environmental dataset we used. Sea Surface Temperature (SST; °C) originated from the NOAA OI SST V2 high resolution dataset provided by the Earth System Research Laboratory, Physical Science Division, Boulder Colorado, USA. Mixed Layer Depth (MLD; m) was provided by the Copernicus Marine Environment Monitoring service (CMEMS) and originated from the Global Ocean Physical Reanalysis product (GLOBAL_REANALYSIS_ PHY_001_030). We used the MLD as a proxy of turbulence level (the deeper the MLD is, the more active the wind-induced turbulence is likely to be) and stratification (a lower

MLD is in general associated with a higher stratification, which prevents nutrients recycling to the surface).

Phosphate, silicate and nitrate concentrations (mmol.m^{-3}) were provided by the CMEMS and came from the Global Ocean Biogeochemistry Hindcast (GLOBAL_REANALYSIS_BIO_001_029). Photosynthetically Active Radiation (PAR; mole /m^2/day) was provided by Globcolour Hermes. PAR was estimated from satellites data. Euphotic depth of sea water (m) was provided by the NASA Goddard Space Flight Center, Ocean Ecology Laboratory, Ocean Biology Processing Group. Euphotic depth was calculated with Lee algorithm. Bathymetry (m) was provided by the British Oceanographic Data Centre (BODC). Distance to nearest coastlines (km) was provided by the Nasa's Ocean Biology Processing Group, Goddard Space Flight Center.

We calculated a daily climatology for each environmental parameter in the North Sea (Figure 2b-h and Supplementary Figures S1 and S2a-c), based on the time period 1997-2017. The climatology of the euphotic depth of sea water was based on the time period 2002-2017. Here also, we based our climatologies on 366 days to match the diatom climatologies. We assumed that the difference of time periods between biological (1958-2017) and environmental (1997-2017) datasets did not alter our conclusions because the seasonal changes observed here, are much more important than decadal changes (see Figure 4). The use of the full time period for CPR data was important to have a more reliable daily climatology and we know that daily variability is much higher than decadal variability, an assumption that has been checked for copepod biodiversity assessed from the CPR data (Beaugrand et al., 2003).

The kinematic viscosity (in $m^2.s^{-1}$) was assessed from SST daily climatology using equations from Pilson (Pilson, 2013) and assuming a salinity of 35 (i.e. mean salinity of the North Sea).

Data on monthly long-term changes in SST (°C), mean surface downward short-wave radiation flux ($W.m^{-2}$), and northward and eastward wind components ($m.s^{-1}$) originated from the ERA5 dataset. This monthly gridded dataset, which covered the period 1958-2017, were provided by the Copernicus climate change service. Data on mean surface downward short-wave radiation flux (solar radiations) were used as a proxy of PAR.

2.3. Morphological traits

2.3.1. Cell shape

We gathered together information on the geometrical shape of each species from the Global Diatoms Database (Leblanc et al., 2012). Six different shapes were distinguished: cylinder, cylinder + 2 half spheres, rectangular box, prism on an elliptic base, prism on a parallelogram base and prism on a triangular base (Supplementary Table S1).

2.3.2. Oblates and prolates

We also retrieved information on minimum and maximum cell dimensions (diameter/height or length/width/height depending upon cell shapes). For cylindrical cells, we defined height as the dimension perpendicular to cell diameter. For other geometrical shapes, we first converted them to a cylinder of equivalent size: we calculated the area of the slice perpendicular to cell height (as defined in the database) and estimated the diameter of the equivalent disk (i.e. the disk of equivalent surface). Based on these cell dimensions, we divided diatoms into three groups: (i) oblates (i.e. minimum height < minimum diameter and maximum height < maximum diameter), (ii) prolates (i.e. minimum height > minimum diameter and maximum height > maximum diameter) and (iii) oblates/prolates for the remaining species/taxa, meaning that they can be both oblates and prolates (Supplementary Table S2).

2.3.3. Other morphological indices

Based on mean cell height (h) and diameter (d) (Supplementary Table S2), we estimated the area (s), the volume (v) and the area/volume ratio (sv^{-1}) of each species by assimilating their shape to a cylinder:

$$s_{cylinder} = \pi d \left(\frac{d}{2} + h\right) \quad [1]$$

$$v_{cylinder} = \frac{\pi}{4} d^2 h \quad [2]$$

We assessed an index of cell morphology, which had the advantage to be dimensionless:

$$\delta = msv^{-1} \quad [3]$$

with m the cell maximum linear dimension (i.e. the mean cell diameter or height for oblates and prolates, respectively). δ describes cell attenuation (i.e. reduction of one of the dimensions of the cell volume or cell flattening) and its departure from a sphere (Naselli-Flores et al., 2021).

We estimated the maximum area of light interception normalized by volume (β). For oblates, we calculated the ratio between disk area and volume as follows:

$$\beta_{oblates} = \frac{\pi\left(\frac{d}{2}\right)^2}{v} \quad [4]$$

For prolates, we calculated the ratio between rectangle area (projection of a cylinder on a surface) and volume:

$$\beta_{prolates} = \frac{dh}{v} \quad [5]$$

179

180 **2.4. Predation**

181 We used abundance data of 74 small (≤ 2 mm) and 196 large (> 2 mm) copepods species/taxa
182 collected by the CPR survey in the North Sea (Supplementary Figure S1). We summed the total
183 abundance for small/large copepods in each CPR sample between 1958-2017 and then calculated a
184 daily abundance climatology for small/large copepods. We therefore obtained two vectors of 366
185 days (one vector for small and another for large copepods) with the daily mean abundance for
186 small/large copepods. As above, we applied twice a simple 6-order moving average and standardized
187 the abundance data between 0 and 1 (Supplementary Figure S2c).

188

189 **2.5. Phylogenetical classification**

190 Information on the phylogenetical classification of the 45 diatoms (family, order, superorder,
191 subclasses) was retrieved from the WOrld Register of Marine Species (WORMS)
192 (http://www.marinespecies.org/index.php). (Supplementary Figure S3 and Table S3).

193

194 **2.6. Analyses**

195 *2.6.1. Principal Component Analysis (PCA)*

196 We characterized Annual Diatom Succession (ADS) by applying a standardized PCA on a matrix of
197 daily abundance climatology (366 days) x diatom species (45 species) (Figure 1a). We examined the
198 first three axes (principal components and eigenvectors) of the PCA because a test based on a
199 broken-stick distribution (Legendre and Legendre, 1998) revealed that the first three axes of the PCA
200 were significant, i.e. they were above average eigenvalues calculated by the broken-stick model
201 (Supplementary Table S4). Seasonal changes in diatom abundance were examined by the first three
202 principal components (PCs) and relationships between species were investigated by using the first
203 three normalized eigenvectors, which represented the correlation of the 45 diatoms with the first
204 three PCs. We tested the relationships between the first three principal components and the daily

climatology for SST, euphotic depth, PAR, MLD, mean small/large copepods abundance, viscosity, silicate, phosphate and nitrate concentration by means of a Spearman rank correlation coefficient. The significance of the correlation coefficients was tested by applying a Montecarlo test with 100,000 simulations (Figure 3 and Supplementary Table S5).

2.6.2. Clustering

We applied a cluster analysis based on the first three normalized eigenvectors of the PCA. First, we calculated a squared matrix of Euclidean distance using the first three eigenvectors. Then we applied a Ward linkage algorithm (Legendre and Legendre, 1998). The resulting dendrogram was cut using a threshold of Euclidean distance of 8; this threshold was chosen because it enabled the identification of three species groups that closely matched the seasonal patterns exhibited by the first three PCs (Figure 1a, 3 and Supplementary Figures S2d-f, S4 and S5).

2.6.3. Relationships between phenology and morphological traits

We examined the relationships between the species groups and morphological traits in the space defined by the first three eigenvectors: (i) geometrical shapes (Figure 1b), (ii) oblates/prolates (Figure 1c), (iii) height-diameter difference (Figure 1d), (iv) area/volume ratio (Figure 1e), (v) δ (Figure 1f), (vi) mean cell diameter (Supplementary Figure S6a) and (vii) mean cell height (Supplementary Figure S6b).

We tested the differences in the mean of the morphological indices (height-diameter (Supplementary Table S6), mean cell diameter (Supplementary Table S7), mean cell height (Supplementary Table S8), area/volume ratio (Supplementary Table S9) and δ (Supplementary Table S10)) among species groups by means of a Kruskal-Wallis test and post-hoc tests.

2.6.4. Comparison between morphological traits based on cylindrical and spheroidal shapes

In our analyses, we assimilated diatom shapes to cylinders. To test whether our conclusions were affected by this assumption, we also compared our results with those obtained by assimilating diatom shapes to spheroids. Based on mean cell height (h) and diameter (d) (Supplementary Table S2), we re-estimated the area (s), the volume (v) and the area/volume ratio (sv^{-1}) of each species by assimilating their shape to spheroids as follows:

$$s_{spheroid} = \frac{\pi d}{2}\left(d + \frac{h^2}{\sqrt{h^2-d^2}}\sin^{-1}\frac{\sqrt{h^2-d^2}}{d}\right) \quad [6]$$

$$v_{spheroid} = \frac{\pi}{6}d^2h \quad [7]$$

We examined the relationships between morphological traits (area, volume, area/volume ratio and δ) when cells were based on cylinders (see equations 1-3) and spheroids by means of Pearson correlation coefficients (Supplementary Figure S7a-d).

We also investigated the relationships between species groups and morphological traits estimated with spheroidal shape in the space defined by the first three eigenvectors using (i) area/volume ratio and (ii) δ (Supplementary Figure S7e-h).

Finally, we tested the differences in the mean of the morphological indices among species groups, based on spheroidal shapes for area/volume ratio (Supplementary Table S11) and δ (Supplementary Table S12), by means of a Kruskal-Wallis test and post-hoc tests.

2.6.5. Relationships between morphological indices and the environment

We also examined the relationships between m and area/volume ratio (Figure 1g-h), PAR and β (Supplementary Figure S8), MLD and δ (Supplementary Figure S9), kinematic viscosity and δ

(Supplementary Figure S10) and between copepod abundance and height-diameter difference (Supplementary Figure S11).

We calculated the Spearman rank correlation coefficient between m and area/volume ratio (Figure 1g), PAR and β (Supplementary Figure S8), MLD and δ (Supplementary Figure S9), kinematic viscosity and δ (Supplementary Figure S10) and between copepod abundance and height-diameter difference (Supplementary Figure S11). The correlations were tested by means of a Montecarlo test using 100,000 permutations (Jackson and Somers, 1989).

2.6.6. Phenology and niche

We estimated the optimum and amplitude (breadth) of the niche using nine ecological dimensions: SST, euphotic depth, PAR, MLD, silicate phosphate and nitrate concentration, bathymetry and distance to nearest coastlines. To do so, we estimated the weighted mean as a proxy for optimum (X_{opt}) and the weighted standard deviation as a proxy for the amplitude (σ) (Figure 2 and Supplementary Figure S12). These proxies were calculated for each ecological dimension:

$$X_{opt} = \frac{\sum_{i=1}^{t} w_i x_i}{\sum_{i=1}^{t} w_i} \quad [8]$$

$$\sigma = \frac{\sum_{i=1}^{t} w_i \left(x_i - x_{opt}\right)^2}{\frac{t-1}{t} \sum_{i=1}^{t} w_i} \quad [9]$$

where w is the abundance of the diatom species, x the value of the environmental parameter or copepod abundance and t the number of days in the climatology (for SST, euphotic depth, PAR, MLD, silicate phosphate and nitrate concentration, and small/large copepod abundance) or the total number of CPR samples when bathymetry or distance to nearest coastlines was used.

We examined the relationships between diatom niche optimum/amplitude, their day of maximum abundance and the daily climatology for SST, euphotic depth, PAR, MLD, silicate phosphate and nitrate concentration (Figure 2b-h). We also investigated the relationships between diatom niche optimum/amplitude and height-diameter difference (Supplementary Figure S12).

We tested the niche separation between oblates and prolates by means of a Krukal-Wallis test performed on niche optima and amplitude (Supplementary Tables S13-S14). The relationships between species niche optima/amplitudes and species height-diameter difference was examined by applying a Spearman rank correlation coefficient and tested with a Montecarlo test using 100,000 simulations (Supplementary Figure S12)(Jackson and Somers, 1989).

2.6.7. Long-term changes in the abundance of oblates and prolates

We investigated long-term monthly changes in the mean abundance of oblates and prolates collected by the CPR survey between 1958 and 2017 (Figure 4a). Oblate abundance in April and October and prolate abundance in August were smoothed by means of a second-order simple moving average (Figure 4b-d). The relationships between species abundance (in April and October for oblates and August for prolates) and the long-term changes in SST, wind and solar radiations were examined by applying a Spearman rank correlation coefficient and tested with a Montecarlo test using 100,000 simulations (Supplementary Table S15)(Jackson and Somers, 1989).

3. Results and Discussion

We first characterised ADS by means of a Principal Component Analysis (PCA) performed on a matrix of daily abundance climatology (366 days) x diatom species (45 species; Methods). The abundance matrix originated from data collected by the Continuous Plankton Recorder (CPR) survey between 1958 and 2017 in the North Sea (Supplementary Figure S1). We retained the first three Principal Components (PCs), which were significant after applying a broken-stick test (Methods and

307 Supplementary Table S4). The first PC (26% of the total variance) showed a strong peak in spring at a
308 time of weak stratification and low temperature, reflecting the spring bloom, and a smaller peak in
309 late autumn at a time of decreasing temperature and stratification breakdown (Caracciolo et al.,
310 2021) (Figure 1a). The second PC (25%) exhibited a similar pattern with two peaks, the lowest in
311 spring and the highest in autumn, again reflecting both spring and autumn blooms. The third PC
312 (15%) showed high positive values from late spring to the end of summer, identifying diatoms that
313 were dominant during the stratified low-nutrients period at a time of higher zooplankton abundance
314 (Supplementary Figure S2a-c). We therefore identify three key periods in ADS, confirming a pattern
315 seen in temperate seas (Caracciolo et al., 2021; Colebrook, 1986, 1984).
316

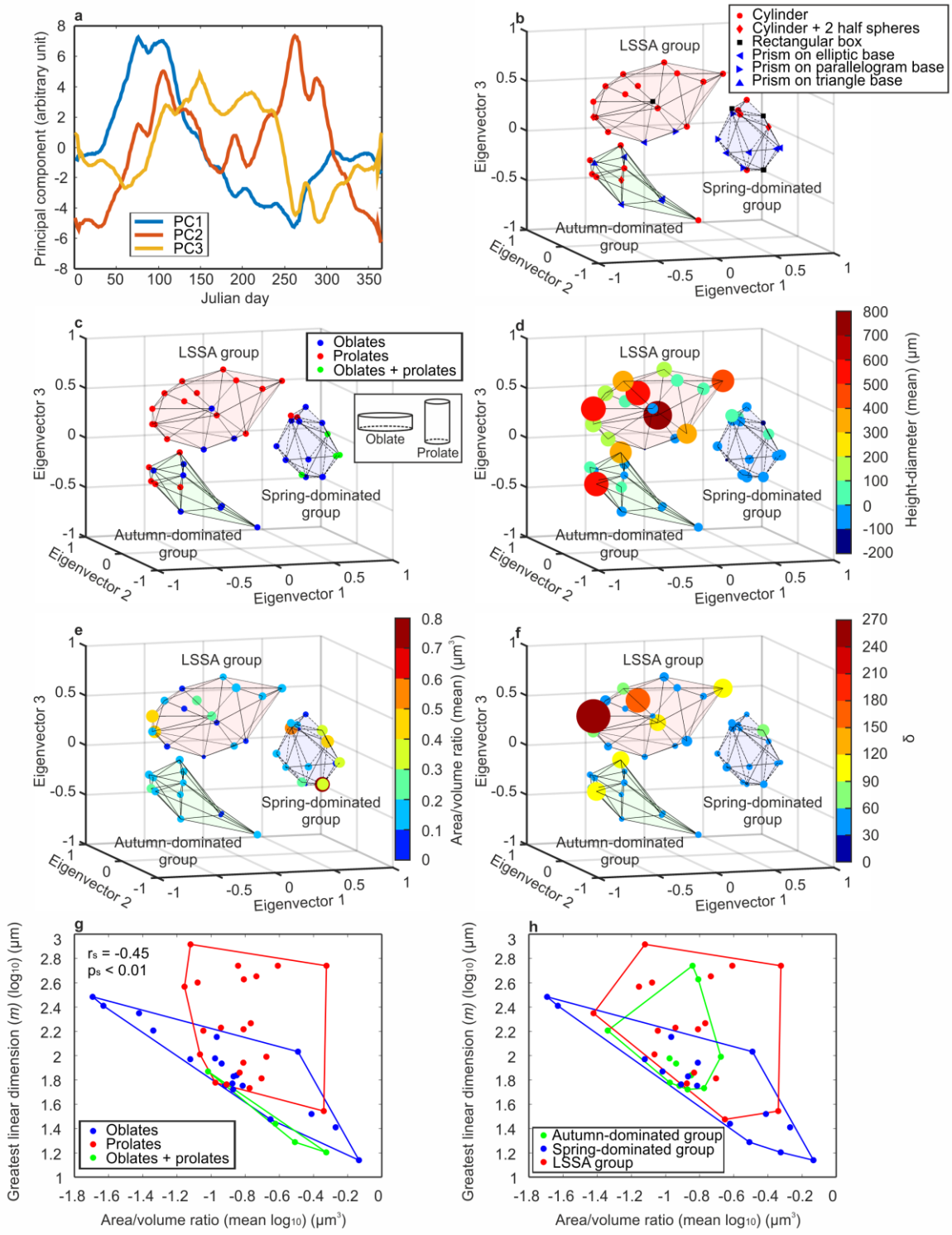

317

318 **Figure 1. Annual Diatom Succession (ADS) and morphological traits.** (**a**) ADS characterized by a PCA
319 applied on a species abundance matrix 366 days x 45 species. The first three principal components
320 (PCs) are shown. (**b-f**) Relationships between the first three eigenvectors and morphological traits.
321 Relationships between species groups and (**b**) morphological traits, (**c**) oblates and prolates, (**d**)
322 height-diameter differences, (**e**) area/volume ratio and (**f**) δ. Blue area delineates the space occupied
323 by the spring-dominated group, green area the space occupied by the autumn-dominated group and
324 red area the space occupied by the LSSA group. (**d-f**) Size and colour of the bullets are scaled with (**d**)
325 mean cell height-diameter difference, (**e**) mean area/volume ratio and (**f**) δ. (**g-h**) Relationships

between cell greatest linear dimension (m)($\log_{10}$) and mean area/volume ratio ($\log_{10}$). Spearman rank correlation coefficient (r_s) and its associated probability (p_s) are displayed on the top left.

We examined species phenology by studying the first three normalised eigenvectors, which represent the correlation between each species and the first three PCs (Figure 1b-f). A cluster analysis, performed on the first three eigenvectors, allowed us to identify three assemblages (Supplementary Figures S2d-f and S4), each belonging to one of the phenological patterns we identified previously (Figure 1b-f): (i) a spring-dominated group related to PC1, (ii) an autumn-dominated group related to PC2 and (iii) a Late-Spring Summer Autumn (LSSA) group related to PC3 (Supplementary Figures S2, S4-S5).

We next studied relationships between species phenology and morphological traits. Cell shape and size are major traits affecting nutrient acquisition, light capture, grazing resistance, and vertical motion (Clifton et al., 2018; Karp-Boss and Boss, 2016; Litchman and Klausmeier, 2008; Naselli-Flores et al., 2021; Naselli-Flores and Barone, 2011; Padisak et al., 2003). To do so, we compiled data on cell size and geometrical shape from the Global Diatom Database (Leblanc et al., 2012) for 45 species/taxa (Methods). Spring-dominated and autumn-dominated groups comprised a mixture of species of different shapes (cylindrical, rectangular box and prism) whereas the LSSA group mainly comprised cylindrical diatoms (Figure 1b and Supplementary Table S1). By assuming all diatom shapes to be cylindrical (note that we also performed the same analyses by assimilating diatom shapes to spheroids, see below), we separated diatoms as oblates (i.e., cell diameter > cell height, flattened cell) and prolates (cell diameter < cell height, elongated cell). We identified 20 oblates and 21 prolates, the remaining being identified as oblates/prolates (i.e. species/taxa that can be both during their life cycle; Methods and Supplementary Table S2). The spring- and autumn-dominated groups mainly comprised oblates (62.5% and 58% in the spring- and autumn-dominated group, respectively; Figure 1c and Supplementary Table S1) and the LSSA group mostly comprised prolates (82%; Figure 1c and Supplementary Table S1).

Following this result, we investigated the variations of the mean cell height-diameter difference between groups more deeply (Figure 1d). Highest and lowest positive differences characterized the LSSA group and the spring-dominated group, respectively. Values were more variable from the autumn-dominated group. A Kruskal-Wallis test revealed significant differences and post-hoc tests showed that differences occurred between LSSA and spring/autumn-dominated groups, but not between spring- and autumn-dominated groups (Supplementary Table S6). Interestingly, negative differences (shown in blue on the colour bar) were smaller than positive ones (from green to red; Figure 1d), suggesting that cell height rather than diameter is modified during ADS; this result is confirmed by insignificant differences in cell diameter and significant differences in cell height among groups (Supplementary Figure S6 and Supplementary Tables S7-S8). Previous studies have suggested that the size of phytoplankton is rarely greater than 300 µm (Naselli-Flores and Barone, 2011) because of fundamental structural constraints imposed by natural selection, i.e. limited minimum thickness and maximum diameter. For example, to avoid turbulence-induced damage and to benefit from the viscosity of water, planktonic cells have to remain smaller than the Kolmogorov scale (i.e. micro eddies) (Naselli-Flores et al., 2021; Reynolds, 1998) and the area/volume ratio needs to remain relatively low to ensure chemical exchanges between the cell and its environment (Raven et al., 2005).

Phytoplankton exhibit different cell shapes that modify their area/volume ratio to optimize nutrient exchange and buoyancy with their surrounding environment (Karp-Boss and Boss, 2016; Pahlow et al., 1997). Energy flux occurs through the cell surface while metabolism is related to the cell volume, which explains why the ratio between surface area and volume should be high, although the building of a large surface has also a negative metabolic cost (Brown et al., 2004). We did not find any significant seasonal changes in the ratio between surface area and volume amongst our three groups (Figure 1e and Supplementary Table S9). Similar results have been documented in tropical lakes and

coastal marine waters where the area/volume ratio was preserved through morphological changes (Lewis, 1976; Stanca et al., 2013). We tested whether elongation (i.e. an increase in the maximum linear dimension or m) could be a more relevant parameter. To do so, we used an index of cell morphology δ (i.e. m times the area/volume ratio; Methods)(Naselli-Flores et al., 2021). In contrast to the area/volume ratio (Figure 1e), we found significant differences in cell morphology (δ) among the three groups (Figure 1f and Supplementary Table S10). Assimilating diatom shapes to spheroids led to similar conclusions (Supplementary Figure S7 and Tables S11-S12). A closer look on m versus sv^{-1} allowed a better understanding of why there was no significant change in the area/volume ratio (Figure 1g-h). The two figures suggest that the dominance of prolates in the LSSA group during the stratified low-nutrients period does not affect the area/volume ratio in contrast to oblates where changes in size do influence the area/volume ratio. These results suggest that cell elongation is a way of altering shape without changing the area/volume ratio that would otherwise affect nutrient exchange (Karp-Boss and Boss, 2016; Pahlow et al., 1997).

Further, we examined whether phylogeny (from family to subclass level) was responsible for the observed differences in traits. We found no evidence for a phylogenetic effect at the family, order and superorder levels. This was not so at the subclass level; although the LSSA and autumn-dominated groups were mainly composed of *Coscinodiscophycidae,* the spring-dominated group was characterized by a diversity of subclasses (Supplementary Figure S3 and Table S3). This analysis, therefore, shows that differences in morphological traits are also influenced by phylogeny. Other studies have suggested that major morphological traits that drive strategies in nutrient uptake are conserved over evolutionary time at a high phylogenetic level, a phenomenon known as trait conservatism (Litchman et al., 2007). Trait conservatism results from stabilizing selection and niche conservatism, i.e. species keeping the shape of their niche unaltered over time because of their propensity to remain in places where the environment is highly suitable for them (Ackerly, 2003).

(Not all phytoplankton traits exhibit the same level of conservatism, some being more labile than others. (Litchman et al., 2010; Schwaderer et al., 2011)).

Three other hypotheses could also explain the morphological changes we observed: (i) light capture optimization (Naselli-Flores and Barone, 2011), (ii) buoyancy (Naselli-Flores et al., 2021; Naselli-Flores and Barone, 2011; Padisak et al., 2003) and (iii) response to predation (Smetacek, 2001). We investigated relationships between maximum area of light interception normalized by volume (β) and Photosynthetically Active Radiation (PAR) (Methods, Supplementary Figure S8). We found no clear relationship between PAR and β. Noticeably, β diminished when maximum PAR increased, which is in agreement with physiology (Reynolds, 1989). However, small values of β were observed for a large range of PARs, which suggests that changes in β are not modulated by PAR for most species considered here. We acknowledge that physiological processes by which the cell can adapt to different light intensity are complex, however (e.g. photosynthetic pigments, see Supplementary Text S3)(Reynolds, 1989).

Many other studies have provided evidence that variations in cell shape might result from an adaptation to turbulence through a modification in sinking velocity (Clifton et al., 2018; Margalef, 1978; Naselli-Flores et al., 2021; Naselli-Flores and Barone, 2011; Padisak et al., 2003). We tested this hypothesis by investigating the relationship between Mixed Layer Depth (MLD, used as a proxy for wind-induced turbulence intensity) and δ (Supplementary Figure S9, Methods). This analysis revealed a negative relationship between maximum MLD values and δ. While oblates were found for a large range of MLDs, prolates dominated low-turbulence waters. We therefore concluded that diatom elongation observed during ADS may result mainly from an adaptation to buoyancy, although resource acquisition and predation probably also play a role (Karp-Boss and Boss, 2016; Pahlow et al., 1997; Sommer, 1998).

Studies have also found negative relationships between temperature and phytoplankton sinking velocity through an alteration in viscosity (Smayda, 1970; Sournia, 1982). From Stokes' equation, and considering a cell of 20 µm of diameter, sinking velocity increases of 4% for each increase of 1°C because of a decrease in viscosity (Smayda, 1970). However, sinking velocity depends on cell shapes (Padisak et al., 2003; Smayda, 1970; Sournia, 1982). We therefore tested the relationship between kinematic viscosity and δ and found a weak but significant negative relationship (Supplementary Figure S10; Methods). This result suggests that prolates may also occur in stratified warm waters because their shapes slow down sinking velocity (Padisak et al., 2003). We acknowledge that we have not considered all processes that can impact phytoplankton buoyancy. First, many species produce organic substances that increase the viscosity of the surrounding environment and that may then trigger cell aggregation, sometimes associated with minerals and particles, which may ultimately increase sinking velocity (Smayda, 1970; Smetacek, 1985). Second, phytoplankton cells can also develop protuberances such as spines and setae that directly increase the frictional drag or help turn the longest cell dimension perpendicular to the settling axis (Padisak et al., 2003; Smayda, 1970). Third, some species form chains that may affect sinking speed, although contrasting results have been observed for different species with either an increase or a decrease in buoyancy (Padisak et al., 2003; Smayda, 1970). Lastly, we have not considered intra-specific variations in size and seasonal morphological plasticity, which can be important in many species (Ligowski et al., 2012).

Lastly, we investigated whether there is a relationship between diatom shape and predation. We examined the relationship between the abundance of small (≤2mm)/large(>2mm) copepods and morphological shape (Methods, Supplementary Figure S11). Although correlation cannot imply causation, we found a nonlinear positive correlation between zooplankton abundance for small and large copepods and height-diameter difference. This result is in agreement with works that have suggested that changes in diatom shape may be influenced by zooplankton predation (Karp-Boss and Boss, 2016; Naselli-Flores and Barone, 2011; Smetacek, 2001), although other works have shown that

456 elongated cells can be ingested by copepods when turbulence is low (Visser and Jonsson, 2000). We
457 caution that defence mechanisms in diatoms are diverse, ranging from physiological (allelopathy) to
458 phenomena such as colony formation and escape response (Pančić and Kiørboe, 2018) and that all
459 mechanisms involved could not be realistically tested in this study.
460
461 Recent works have suggested that annual plankton succession results from the niche-environment
462 interaction (Caracciolo et al., 2021). We therefore explored the relationships between cell shape and
463 ecological niche for the 45 species/taxa. Here, the ecological niche was characterised by its optimum
464 and amplitude (i.e. niche breadth) (Hutchinson, 1957); these niche parameters were assessed for
465 each species/taxa and nine environmental parameters (Methods; Figure 2a). Our results suggest that
466 morphological traits influence species' niche of diatoms and that oblates and prolates had significant
467 differences in ecological optima for all niche dimensions. Amplitudes were also distinct for four niche
468 dimensions: nutrients (nitrate, phosphate and silicate) and MLD (Figure 2b-h, Supplementary Tables
469 S13-S14). Although the relationship was less obvious for sea surface temperature and euphotic depth
470 (Figure 2b-c), optima and amplitudes plotted against daily climatology of each parameter showed a
471 clear dominance of prolates during low-nutrients, turbulence and PAR conditions (Figure 2d-h). In
472 addition, oblates were significantly more euryoecious (i.e. larger niche amplitude) than prolates with
473 respect to nutrients and MLD (Figure 2e-h, Supplementary Figure S12 and Table S14). Prolates are
474 therefore K-strategists (i.e. equilibrium species), adapted to stable environment (i.e. predictable
475 environment with low perturbations) with respect to nutrients, turbulence and stratification (low
476 MLD) whereas oblates are more r-strategists (i.e. opportunist species), adapted to a more unstable
477 environment (i.e. unpredictable) (Southwood et al., 1974). In other words, prolates (K-strategist)
478 thrive in stratified water with low turbulence and constant low-nutrient concentration whereas
479 oblates (r-strategists) thrive in turbulent waters in the absence of stratification with more variable
480 levels of nutrients concentration (Figure 2). Because oblates and prolates have distinct niches, this
481 analysis demonstrates that morphological traits influence species niche and phenology. We

summarize the relationships between diatom morphological traits, phenology and the environment in Figure 3 (see also Supplementary Table S5).

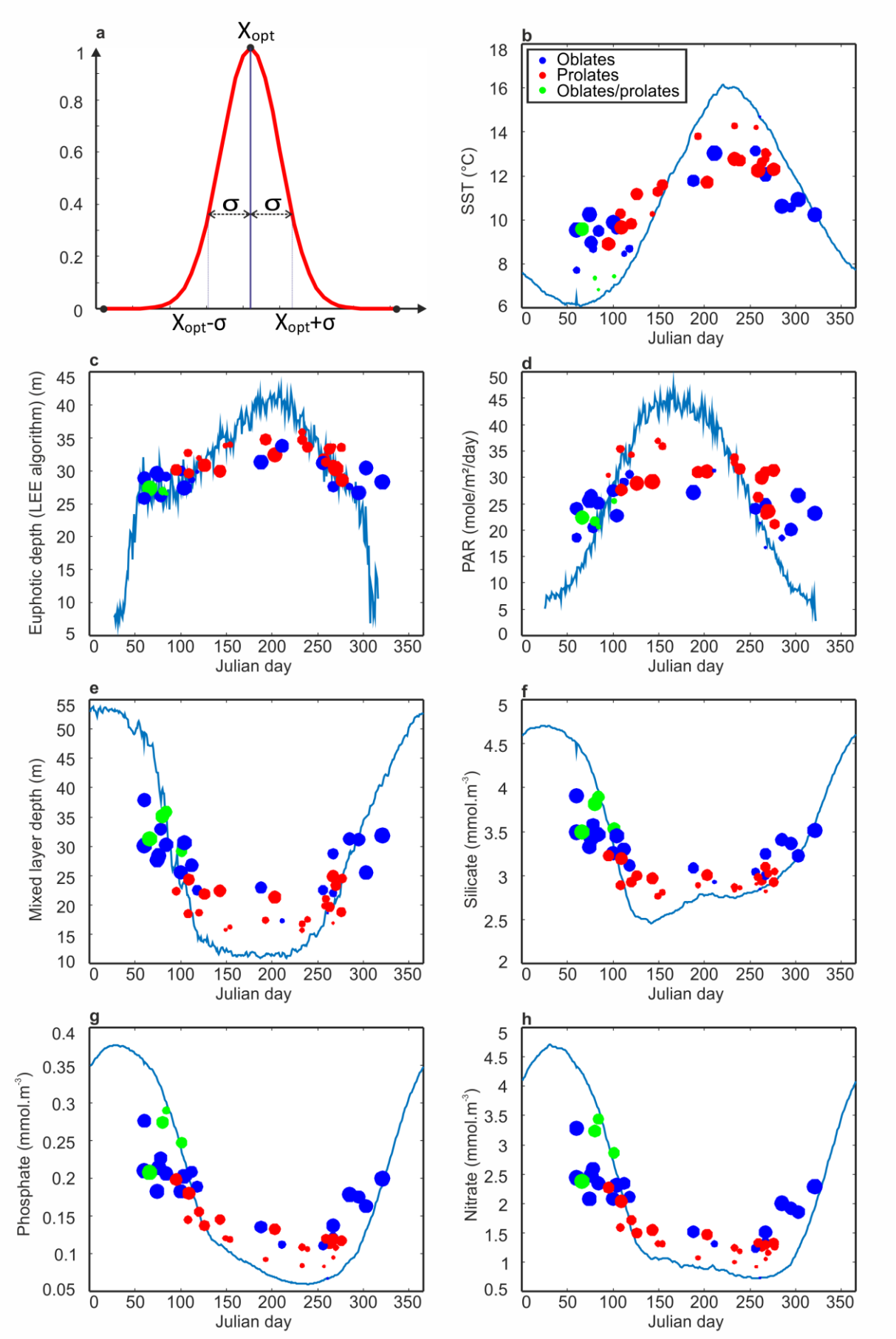
a
X_{opt}
σ
σ
X_{opt}-σ
X_{opt}+σ
b
Oblates
Prolates
Oblates/prolates
SST (°C)
Julian day
c
Euphotic depth (LEE algorithm) (m)
Julian day
d
PAR (mole/m²/day)
Julian day
e
Mixed layer depth (m)
Julian day
f
Silicate (mmol.m^{-3})
Julian day
g
Phosphate (mmol.m^{-3})
Julian day
h
Nitrate (mmol.m^{-3})
Julian day

485

Figure 2. Relationships between day of maximum abundance and ecological optima/amplitude of each diatom and environmental parameter. (**a**) Theoretical ecological niche with X_{opt} representing species niche optimum and σ denoting niche amplitude assessed by the weighted standard deviation. The Y axis corresponds to the species abundance and the X axis to an hypothetical environmental parameter. Relationships between day of maximum abundance and niche optimum/amplitude for (**b**) SST, (**c**) euphotic depth, (**d**) PAR, (**e**) mixed layer depth (MLD), (**f**) silicate, (**g**) phosphate and (**h**) nitrate concentration. Blue lines correspond to the North Sea daily climatology of the parameter considered in the panel. The niche optimum can be read on the ordinate axis. The size of the bullet is a function of species' rank of the weighted standard deviation; larger bullets are associated with larger niche amplitude and therefore ranks. Oblates are in blue, prolates in red and oblates/prolates in green.

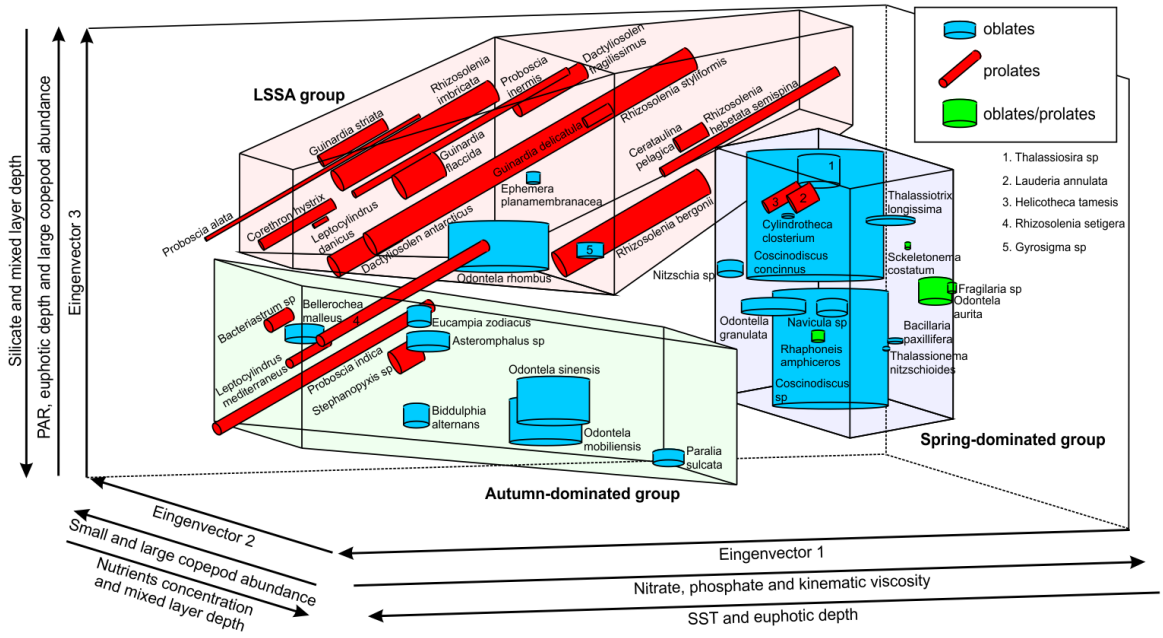

Figure 3. Summary of the relationships between the first three eigenvectors, diatom shapes and the environment. Cell shapes are represented by cylinders scaled with species height and diameter (Supplementary Table S2). Oblates are in blue, prolates in red and oblates/prolates in green. Species names are those recorded in the CPR dataset. Blue area delineates the space occupied by the spring-dominated group, green area the space occupied by the autumn-dominated group and red area the space occupied by the LSSA group. Correlation between the first three principal components and the environmental parameters are displayed in Supplementary Table S5. More information on the principal components can be found in Figure 1a.

Finally, we investigated long-term monthly changes in the abundance of oblates and prolates between 1958 and 2017. Our results show that both groups exhibit distinct patterns of temporal changes (Figure 4a), with oblates having a constant and high level of abundance in April (Figure 4b) but a more variable abundance in October with blooms of decreasing intensity during the 1960s and 1970s, followed by a strong increase after *circa* 1980 (Figure 4c). Similar patterns are also observed

for prolates in August but with an abundance level below the maximum reached in 1960 (Figure 4d). The period of low abundance found for oblates and prolates between 1978 and 1982 was probably the consequence of a cold hydro-meteorological anomaly observed in the North Sea (Edwards et al., 2002). We subsequently investigated whether these long-term changes in abundance were correlated with long-term changes in Sea Surface Temperature (SST), wind and solar radiations (Supplementary Table S15). We found a nonlinear positive correlation between oblate abundance in October and SST and a negative correlation with eastward wind as well as wind intensity. A negative correlation was also found between oblate abundance in April and eastward wind. No significant correlations with northward wind and solar radiations were found. In the Northeast Atlantic region, long-term changes in SST/wind variations have led to a marked increase in diatoms, associated with a diminution in dinoflagellates (Hinder et al., 2012).

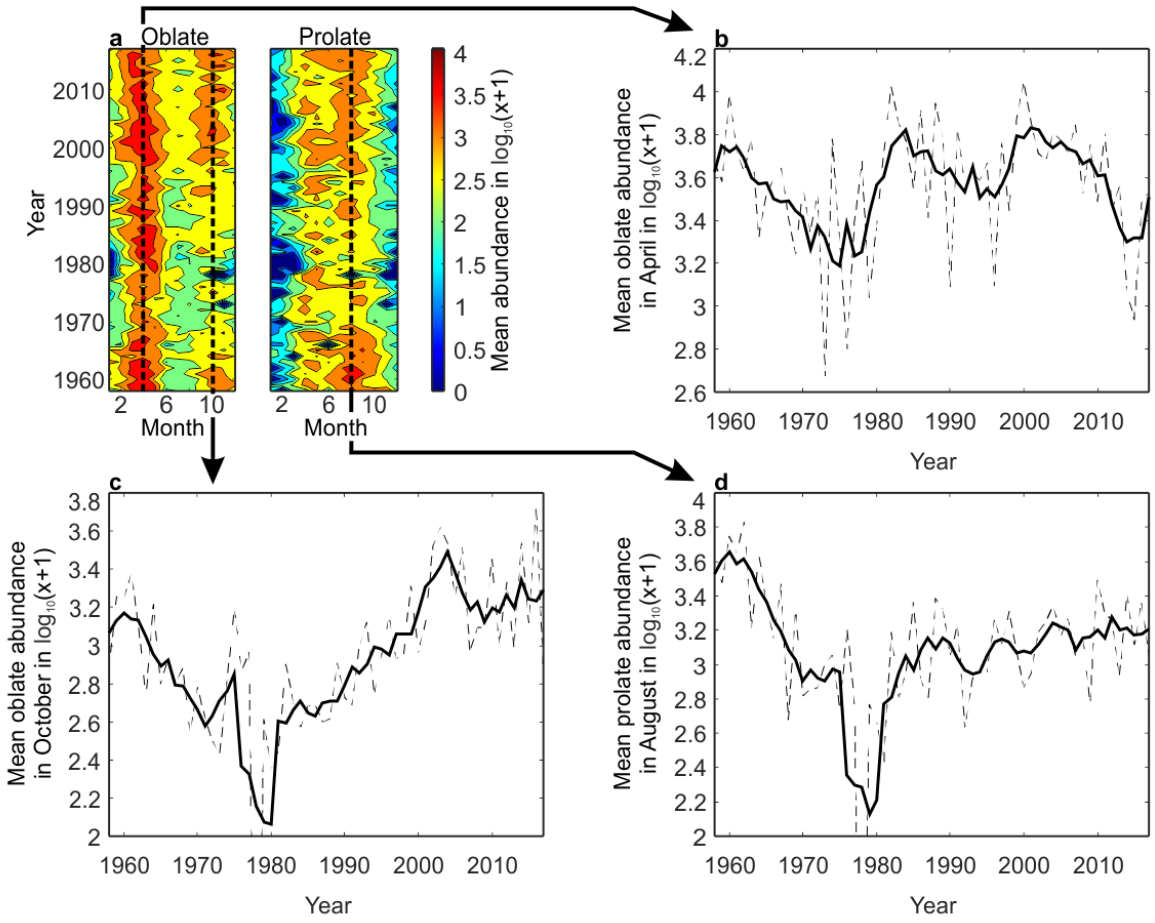

Figure 4. Long-term changes in oblate and prolate abundance (i.e. number per CPR sample) between 1958 and 2017. (**a**) Long-term monthly changes in total oblate and prolate abundance. Dashed lines highlight the months that were considered in the examination of long-term changes in oblates or prolates on panels (**b**), (**c**) and (**d**). (**b**-**d**) Long-term changes in the abundance of oblates in (**b**) April and (**c**) October and (**d**) of prolates in August. Dashed lines represent the long-term changes in diatom abundance from panel (**a**) and black bold lines show the smoothed long-term changes after applying a second-order simple moving average. Note that the exceptional nil abundance value observed for oblates and prolates in 1978 is below the y axis in the panels **c** and **d**.

Because oblates and prolates exhibit specific long-term changes, our results suggest they may respond to different environmental forcing. However, it is widely assumed that diatom contribution to primary production and carbon export will decline in the mid and low latitudes because ocean warming will increase stratification and decrease nutrients supply to the surface ocean (Bopp et al., 2013, 2005; Dutkiewicz et al., 2013; Fu et al., 2016). Such predictions are made because of an oversimplification of Margalef's mandala (Margalef, 1978) assimilating diatoms to a single Plankton Functional Type (PFT) that thrives when nutrients and turbulence are high (Fu et al., 2016; Kemp and Villareal, 2018; Tréguer et al., 2018). Therefore, current state-of-the-art biogeochemical models only consider oblates in their simulations and not prolates, but our results clearly show that diatoms, through morphological adaptations, are able to exploit a wider range of environment, which is also confirmed by (i) a *Tara* Oceans expedition study that has found comparable diatom diversity in oligotrophic and coastal regions (Malviya et al., 2016) and by (ii) fossil records of the Mediterranean sea, where sapropels (one of the most carbon-rich sediments) formation is associated with highly stratified conditions and high diatom production and export (Kemp and Villareal, 2013). Hence, we suggest that biogeochemical and earth-system models should consider diatom morphology by defining two PFTs (i.e. oblates and prolates) in their settings to improve their predictions on the consequences of climate change on primary production and carbon export.

4. Conclusions

By characterizing ADS in the North Sea with a trait-based approach, we have shown that this phenomenon is controlled by the niche-environment interaction that results from seasonal changes

556 in morphological traits. Although four different hypotheses have been proposed to explain changes
557 in cell shapes (Karp-Boss and Boss, 2016; Litchman and Klausmeier, 2008; Naselli-Flores et al., 2021;
558 Naselli-Flores and Barone, 2011; Smetacek, 2001), our results suggest that cell adaptation to
559 turbulence and viscosity is of primary importance. Cell elongation gives a competitive advantage to
560 diatoms in low-turbulence and low-viscous waters because it diminishes sinking velocity (Padisak et
561 al., 2003). Our results have also shown that elongation does not affect surface/volume ratio and
562 therefore the ability of cells to absorb nutrients (Figure 1g-h). We did not find any evidence that
563 elongation might enhance light capture despite some suggestions that it might (Naselli-Flores and
564 Barone, 2011). Finally, although some studies have suggested that zooplankton can feed on large
565 chains and elongated cells (Djeghri et al., 2018; Visser and Jonsson, 2000), the positive correlation
566 between copepod abundance and elongation that we found suggests predation may also be an
567 important selective agent. Our study suggests that prolates and oblates are key adaptations to
568 specific environments, conferring to species a specific niche. The resulting niche-environment
569 interaction explains phenology and therefore the precise position of a species in the sequence of
570 ADS. Understanding the relationships between morphological traits and species niche can help us to
571 better anticipate community shifts and their functional implications for the ecosystems in the
572 context of global climate change (Litchman et al., 2012). To conclude, as both oblates and prolates
573 exhibit different long-term changes in abundance, suggesting that they might also have different
574 responses to climate forcing, we encourage biogeochemical and earth-system modelers to
575 implement these two diatom groups to improve the assessment of marine primary production and
576 carbon export.
577
578 **Acknowledgements:** We would like to thank the owners and crews that have towed the CPRs on a
579 voluntary basis for over 80 years contributing to one of the world's largest and longest ongoing
580 ecological experiments. Without these early pioneers of citizen science and broad-scale volunteer
581 monitoring projects this unique ecological dataset would never have been financially or logistically

viable. The authors also want to thanks Eric Lecuyer, Dimitra-Ioli Skouroliakou, Monica Michel-Rodriguez and Lucie Courcot for their helpful comments during the design of this study.

Data sharing statement: Data used in the production of this manuscript are already freely available (see Materials and Methods section and Supplementary Text S2).

Funding information: This work is supported by the Centre National de la Recherche Scientifique (CNRS), the Region Hauts-de-France and the Marine Biological Association of the UK.

References

Ackerly, D.D., 2003. Community Assembly, Niche Conservatism, and Adaptive Evolution in Changing Environments. Int. J. Plant Sci. 164, S165–S184. https://doi.org/10.1086/368401

Beaugrand, G., Brander, K.M., Lindley, J.A., Souissi, S., Reid, P.C., 2003a. Plankton effect on cod recruitment in the North Sea. Nature 426, 661–664. https://doi.org/10.1038/nature02164

Beaugrand, G., Ibañez, F., Lindley, J.A., 2003b. An overview of statistical methods applied to CPR data. Prog. Oceanogr. 58, 235–262. https://doi.org/10.1016/j.pocean.2003.08.006

Behrenfeld, M.J., 2010. Abandoning Sverdrup's Critical Depth Hypothesis on phytoplankton blooms. Ecology 91, 977–989. https://doi.org/10.1890/09-1207.1

Bopp, L., Aumont, O., Cadule, P., Alvain, S., Gehlen, M., 2005. Response of diatoms distribution to global warming and potential implications: A global model study. Geophys. Res. Lett. 32. https://doi.org/10.1029/2005GL023653

Bopp, L., Resplandy, L., Orr, J.C., Doney, S.C., Dunne, J.P., Gehlen, M., Halloran, P., Heinze, C., Ilyina, T., Séférian, R., Tjiputra, J., Vichi, M., 2013. Multiple stressors of ocean ecosystems in the 21st century: projections with CMIP5 models. Biogeosciences 10, 6225–6245. https://doi.org/10.5194/bg-10-6225-2013

Brown, J.H., Gillooly, J.F., Allen, A.P., Savage, V.M., West, G.B., 2004. Toward a metabolic theory of ecology. Ecology 85, 1771–1789. https://doi.org/10.1890/03-9000

Caracciolo, M., Beaugrand, G., Hélaouët, P., Gevaert, F., Edwards, M., Lizon, F., Kléparski, L., Goberville, E., 2021. Annual phytoplankton succession results from niche-environment interaction. J. Plankton Res. 43, 85–102. https://doi.org/10.1093/plankt/fbaa060

Chivers, W.J., Walne, A.W., Hays, G.C., 2017. Mismatch between marine plankton range movements and the velocity of climate change. Nat. Commun. 8, 14434. https://doi.org/10.1038/ncomms14434

Clifton, W., Bearon, R.N., Bees, M.A., 2018. Enhanced sedimentation of elongated plankton in simple flows. IMA J. Appl. Math. 83, 743–766. https://doi.org/10.1093/imamat/hxy024

Colebrook, J.M., 1986. Environmental influences on long-term variability in marine plankton. Hydrobiologia 142, 309–325.

Colebrook, J.M., 1984. Continuous plankton records: relationships between species of phytoplankton and zooplankton in the seasonal cycle. Marine Biology 83, 313–323.

Cushing, D.H., 1990. Plankton Production and Year-class Strength in Fish Populations: an Update of the Match/Mismatch Hypothesis. Adv. Mar. Biol. 26, 249–293. https://doi.org/10.1016/S0065-2881(08)60202-3

624 Djeghri, N., Atkinson, A., Fileman, E.S., Harmer, R.A., Widdicombe, C., McEvoy, A.J., Cornwell, L.,
625 Mayor, D.J., 2018. High prey-predator size ratios and unselective feeding in copepods: A
626 seasonal comparison of five species with contrasting feeding modes. Prog. Oceanogr. 165,
627 63–74. https://doi.org/10.1016/j.pocean.2018.04.013
628 Dutkiewicz, S., Scott, J.R., Follows, M.J., 2013. Winners and losers: Ecological and biogeochemical
629 changes in a warming ocean. Glob. Biogeochem. Cycles 27, 463–477.
630 https://doi.org/10.1002/gbc.20042
631 Edwards, M., Beaugrand, G., Reid, P.C., Rowden, A.A., Jones, M.B., 2002. Ocean climate anomalies
632 and the ecology of the North Sea. Mar. Ecol. Prog. Ser. 239, 1–10.
633 https://doi.org/10.3354/meps239001
634 Edwards, M., Richardson, A.J., 2004. Impact of climate change on marine pelagic phenology and
635 trophic mismatch. Nature 430, 881–884. https://doi.org/10.1038/nature02808
636 Falkowski, P.G., Katz, M.E., Knoll, A.H., Quigg, A., Raven, J.A., Schofield, O., Taylor, F.J.R., 2004. The
637 Evolution of Modern Eukaryotic Phytoplankton. Science 305, 8.
638 Fu, W., Randerson, J.T., Moore, J.K., 2016. Climate change impacts on net primary production (NPP)
639 and export production (EP) regulated by increasing stratification and phytoplankton
640 communitystructure in the CMIP5 models. Biogeosciences 13, 5151–5170.
641 https://doi.org/10.5194/bg-13-5151-2016
642 Hinder, S.L., Hays, G.C., Edwards, M., Roberts, E.C., Walne, A.W., Gravenor, M.B., 2012. Changes in
643 marine dinoflagellate and diatom abundance under climate change. Nat. Clim. Change 2,
644 271–275. https://doi.org/10.1038/nclimate1388
645 Hutchinson, G.E., 1957. Concluding remarks. Cold Spring Harb. Symp. Quant. Biol. 22, 415–427.
646 Jackson, D.A., Somers, K.M., 1989. Are probability estimates from the permutation model of Mantel's
647 test stable? Can. J. Zool. 67, 766–769. https://doi.org/10.1139/z89-108
648 Jin, X., Gruber, N., Dunne, J.P., Sarmiento, J.L., Armstrong, R.A., 2006. Diagnosing the contribution of
649 phytoplankton functional groups to the production and export of particulate organic carbon,
650 $CaCO_3$, and opal from global nutrient and alkalinity distributions. Glob. Biogeochem. Cycles
651 20. https://doi.org/10.1029/2005GB002532
652 Jonas, T.D., Walne, A.W., Beaugrand, G., Gregory, L., Hays, G.C., 2004. The volume of water filtered
653 by a Continuous Plankton Recorder sample: the effect of ship speed. J. Plankton Res. 26,
654 1499–1506. https://doi.org/10.1093/plankt/fbh137
655 Karp-Boss, L., Boss, E., 2016. The Elongated, the Squat and the Spherical: Selective Pressures for
656 Phytoplankton Shape, in: Glibert, P.M., Kana, T.M. (Eds.), Aquatic Microbial Ecology and
657 Biogeochemistry: A Dual Perspective. Springer International Publishing, Cham, pp. 25–34.
658 https://doi.org/10.1007/978-3-319-30259-1_3
659 Katz, M.E., Wright, J.D., Miller, K.G., Cramer, B.S., Fennel, K., Falkowski, P.G., 2005. Biological
660 overprint of the geological carbon cycle. Mar. Geol. 217, 323–338.
661 Kemp, A.E.S., Villareal, T.A., 2018. The case of the diatoms and the muddled mandalas: Time to
662 recognize diatom adaptations to stratified waters. Prog. Oceanogr. 167, 138–149.
663 https://doi.org/10.1016/j.pocean.2018.08.002
664 Kemp, A.E.S., Villareal, T.A., 2013. High diatom production and export in stratified waters – A
665 potential negative feedback to global warming. Prog. Oceanogr. 119, 4–23.
666 https://doi.org/10.1016/j.pocean.2013.06.004
667 Leblanc, K., Arístegui, J., Armand, L., Assmy, P., Beker, B., Bode, A., Breton, E., Cornet, V., Gibson, J.,
668 Gosselin, M.-P., Kopczynska, E., Marshall, H., Peloquin, J., Piontkovski, S., Poulton, A.J.,
669 Quéguiner, B., Schiebel, R., Shipe, R., Stefels, J., van Leeuwe, M.A., Varela, M., Widdicombe,
670 C., Yallop, M., 2012. A global diatom database – abundance, biovolume and biomass in the
671 world ocean. Earth Syst. Sci. Data 4, 149–165. https://doi.org/10.5194/essd-4-149-2012
672 Legendre, P., Legendre, L., 1998. Numerical Ecology. Elsevier, Amsterdam - Lausanne - New York -
673 Oxford - Shannon - Singapore - Tokyo.
674 Lewis, W.M., 1976. Surface/Volume Ratio: Implications for Phytoplankton Morphology. Science 192,
675 885–887. https://doi.org/10.1126/science.192.4242.885

676 Ligowski, R., Jordan, R.W., Assmy, P., 2012. Morphological adaptation of a planktonic diatom to
677 growth in Antarctic sea ice. Mar Biol 11.
678 Litchman, E., de Tezanos Pinto, P., Klausmeier, C.A., Thomas, M.K., Yoshiyama, K., 2010. Linking traits
679 to species diversity and community structure in phytoplankton. Hydrobiologia 653, 15–28.
680 https://doi.org/10.1007/s10750-010-0341-5
681 Litchman, E., Edwards, K.F., Klausmeier, C.A., Thomas, M.K., 2012. Phytoplankton niches, traits and
682 eco-evolutionary responses to global environmental change. Mar Ecol Prog Ser 470, 235–
683 248. https://doi.org/doi: 10.3354/meps09912
684 Litchman, E., Klausmeier, C.A., 2008. Trait-Based Community Ecology of Phytoplankton. Annu. Rev.
685 Ecol. Evol. Syst. 39, 615–639. https://doi.org/10.1146/annurev.ecolsys.39.110707.173549
686 Litchman, E., Klausmeier, C.A., Schofield, O.M., Falkowski, P.G., 2007. The role of functional traits and
687 trade-offs in structuring phytoplankton communities: scaling from cellular to ecosystem
688 level. Ecol. Lett. 10, 1170–1181. https://doi.org/10.1111/j.1461-0248.2007.01117.x
689 Malviya, S., Scalco, E., Audic, S., Vincent, F., Veluchamy, A., Poulain, J., Wincker, P., Iudicone, D., de
690 Vargas, C., Bittner, L., Zingone, A., Bowler, C., 2016. Insights into global diatom distribution
691 and diversity in the world's ocean. Proc. Natl. Acad. Sci. 113, 1516–1525.
692 https://doi.org/10.1073/pnas.1509523113
693 Margalef, R., 1978. Life-forms of phytoplankton as survival alternatives in an unstable environment.
694 Oceanol. Acta 1, 493–509.
695 Naselli-Flores, L., Barone, R., 2011. Invited Review - Fight on Plankton! or, Phytoplankton Shape and
696 Size as Adaptive Tools to Get Ahead in the Struggle for Life. Cryptogam. Algol. 32, 157–204.
697 https://doi.org/10.7872/crya.v32.iss2.2011.157
698 Naselli-Flores, L., Zohary, T., Padisák, J., 2021. Life in suspension and its impact on phytoplankton
699 morphology: an homage to Colin S. Reynolds. Hydrobiologia 848, 7–30.
700 https://doi.org/10.1007/s10750-020-04217-x
701 Nelson, D.M., Tréguer, P., Brzezinski, M.A., Leynaert, A., Quéguiner, B., 1995. Production and
702 dissolution of biogenic silica in the ocean: Revised global estimates, comparison with regional
703 data and relationship to biogenic sedimentation. Glob. Biogeochem. Cycles 9, 359–372.
704 https://doi.org/10.1029/95GB01070
705 Padisak, J., Soroczki-Pinter, E., Rezner, Z., 2003. Sinking properties of some phytoplankton shapes and
706 the relation of form resistance to morphological diversity of plankton – an experimental
707 study. Hydrobiologia 500, 243–257.
708 Pahlow, M., Riebesell, U., Wolf-Gladrow, D.A., 1997. Impact of cell shape and chain formation on
709 nutrient acquisition by marine diatoms. Limnol. Oceanogr. 42, 1660–1672.
710 https://doi.org/10.4319/lo.1997.42.8.1660
711 Pančić, M., Kiørboe, T., 2018. Phytoplankton defence mechanisms: traits and trade-offs: Defensive
712 traits and trade-offs. Biol. Rev. 93, 1269–1303. https://doi.org/10.1111/brv.12395
713 Pilson, M.E.Q., 2013. An Introduction to the Chemistry of the Sea., second edition. ed. Cambridge
714 University Press.
715 Platt, T., Fuentes-Yaco, C., Frank, K.T., 2003. Spring algal bloom and larval fish survival. Nature 423,
716 398–399.
717 Raven, P., Johnson, G., Losos, J., Singer, S., 2005. Biology. Mc Graw-Hill.
718 Reid, P.C., Colebrook, J.M., Matthews, J.B.L., Aiken, J., Continuous Plankton Recorder Team, 2003.
719 The Continuous Plankton Recorder: concepts and history, from Plankton Indicator to
720 undulating recorders. Prog. Oceanogr. 58, 117–173.
721 https://doi.org/10.1016/j.pocean.2003.08.002
722 Reynolds, C.S., 1998. Plants in motion: Physical - biological interaction in the plankton, in: Imberger, J.
723 (Ed.), Coastal and Estuarine Studies. American Geophysical Union, Washington, D. C., pp.
724 535–560. https://doi.org/10.1029/CE054p0535
725 Reynolds, C.S., 1989. Physical determinants of phytoplankton succession, in: Sommer, U. (Ed.),
726 Plankton Ecology Succession in Plankton Communities. Springer-Verlag, Berlin, Heidelberg,
727 New York, London, Paris, Tokyo, p. 377.

Schwaderer, A.S., Yoshiyama, K., de Tezanos Pinto, P., Swenson, N.G., Klausmeier, C.A., Litchman, E., 2011. Eco-evolutionary differences in light utilization traits and distributions of freshwater phytoplankton. Limnol. Oceanogr. 56, 589–598. https://doi.org/10.4319/lo.2011.56.2.0589

Smayda, T., 1970. The suspension and sinking of phytoplankton in the sea. Oceanogr. Mar. Biol. Ann. Rev. 8, 353–414.

Smetacek, V., 2001. A watery arms race. Nature 411, 745.

Smetacek, V., 1985. Role of sinking in diatom life-history cycles: ecological, evolutionary and geological significance. Mar. Biol. 84, 239–251.

Sommer, U., 1998. Silicate and the functional geometry of marine phytoplankton. J. Plankton Res. 20, 1853–1859. https://doi.org/10.1093/plankt/20.9.1853

Sournia, A., 1982. Form and function in marine phytoplankton. Biol. Rev. 57, 347–394.

Southwood, T.R.E., May, R.M., Hassell, M.P., Conway, G.R., 1974. Ecological strategies and population parameters. Am. Nat. 108, 791–804.

Stanca, E., Cellamare, M., Basset, A., 2013. Geometric shape as a trait to study phytoplankton distributions in aquatic ecosystems. Hydrobiologia 701, 99–116. https://doi.org/10.1007/s10750-012-1262-2

Tréguer, P., Bowler, C., Moriceau, B., Dutkiewicz, S., Gehlen, M., Aumont, O., Bittner, L., Dugdale, R., Finkel, Z., Iudicone, D., Jahn, O., Guidi, L., Lasbleiz, M., Leblanc, K., Levy, M., Pondaven, P., 2018. Influence of diatom diversity on the ocean biological carbon pump. Nat. Geosci. 11, 27–37. https://doi.org/10.1038/s41561-017-0028-x

Visser, A.W., Jonsson, P.R., 2000. On the reorientation of non-spherical prey particles in a feeding current. Journal of Plankton Research 22, 761–777.